Original Article

Assessing treatment accuracy of image-guided liver stereotactic body radiotherapy: a quantitative analysis based on 4D CT through post-therapeutic MRI-morphologic alterations

Huiling Ye[1,2#^], Chengchiuyat Chan[1#], Yihan Huang[1], Yuehu Pu[2], Mengya Guo[3], Xiangbin Zhang[1], Yingjie Zhang[1], Xin Wang[4], Jitao Zhou[4], Jiayu Duan[4], Shichao Wang[1], Liqing Peng[5], Hang Yu[1], Qiaoyue Tan[1], Xianhu Zeng[1], Renming Zhong[1^]

[1]Radiotherapy Physics & Technology Center, Cancer Center, West China Hospital, Sichuan University, Chengdu, China; [2]Innovation Institute for Integration of Medicine and Engineering, Med-X Center for Manufacturing, West China Hospital, Sichuan University, Chengdu, China; [3]CT Imaging Research Center, GE Healthcare China, Beijing, China; [4]Department of Abdomen Oncology, West China Hospital, Sichuan University, Chengdu, China; [5]Department of Radiology, West China Hospital, Sichuan University, Chengdu, China

Contributions: (I) Conception and design: R Zhong, H Ye; (II) Administrative support: Y Pu, Y Zhang, X Wang; (III) Provision of study materials or patients: J Zhou, X Zhang, J Duan, X Zeng; (IV) Collection and assembly of data: H Ye, C Chan, Y Huang, L Peng; (V) Data analysis and interpretation: H Ye, S Wang, H Yu, Q Tan, M Guo; (VI) Manuscript writing: All authors; (VII) Final approval of manuscript: All authors.

[#]These authors contributed equally to this work.

Correspondence to: Renming Zhong, PhD. Radiotherapy Physics & Technology Center, Cancer Center, West China Hospital, Sichuan University, 37 Guoxue Lane, Wuhou District, Chengdu 610041, China. Email: zrm_100@163.com.

Background: Stereotactic body radiotherapy (SBRT) has become a promising alternative for patients with inoperable liver cancer. However, the accurate delivery of high doses to moving liver tumors remains challenging. Treatment accuracy can be quantified by comparing post-radiotherapeutic magnetic resonance imaging (MRI)-morphologic alterations (MMA) and corresponding isodose-structure cropped to the liver (ISL) upon planning computed tomography (CT). The study aimed to evaluate the robustness of accuracy metrics, and investigate the factors influencing treatment accuracy of liver SBRT using an internal target volume (ITV) strategy based on four-dimensional (4D) CT.

Methods: A retrospective observational study was conducted on a cohort of 31 liver cancer patients who underwent liver SBRT using an ITV strategy based on 4D CT from October 2018 to March 2024. All patients exhibited localized morphological changes on MRI. In vivo analysis (IVA) of liver SBRT was performed by comparing MMA and ISL following deformable image registration of post-radiotherapeutic MRI and planning CT. Accuracy metrics included Dice similarity coefficient (DSC), conformity index of MMA and ISL (CIMI), Hausdorff distance (HD), mean distance to agreement (MDA), and three-dimensional center-of-mass difference (3D-CoMD). Correlation analysis regarding accuracy metrics and potential factors was conducted to evaluate the robustness of accuracy metrics. Patients were stratified into two groups in ascending order. Kaplan-Meier method was used to evaluate IVA's influence on progression-free survival (PFS) of clinical target volume (CTV) in the two groups. Two-sample *t*-test was used to analysis the difference of motion amplitude in the two groups.

Results: Distance metrics (HD, MDA, and 3D-CoMD) were significantly ($P<0.050$) influenced by gross tumor volume (GTV), planning target volume (PTV), and time to post-therapeutic MRI. Patients with DSC >0.7, CIMI >0.5, HD <25 mm, MDA <5 mm, and 3D-CoMD <8 mm showed significant differences in PFS

^ ORCID: Huiling Ye, 0009-0008-1924-2049; Renming Zhong, 0000-0002-1429-6469.

of CTV (log-rank P=0.013, log-rank P=0.013, log-rank P=0.001, log-rank P=0.009, and log-rank P=0.022, respectively). Motion amplitude did not show significant difference in the two groups defined by thresholds of DSC, CIMI, HD, MDA, and 3D-CoMD.

Conclusions: In this *in vivo* accuracy evaluation, conformity metrics such as the DSC and CIMI were more robust than HD, MDA, and 3D-CoMD. Therefore, DSC and CIMI could be a potential predictor for PFS within CTV. However, motion amplitude could not affect the DSC and CIMI. Therefore, a quality assurance procedure in dose delivery should be applied for the ITV strategy based on 4D CT.

Keywords: Liver cancer; four-dimensional computed tomography (4D CT); *in vivo* accuracy; internal target volume strategy (ITV strategy); stereotactic body radiotherapy (SBRT)

Submitted Oct 28, 2024. Accepted for publication Mar 07, 2025. Published online Apr 28, 2025.
doi: 10.21037/qims-24-2309
View this article at: https://dx.doi.org/10.21037/qims-24-2309

Introduction

Liver cancer poses a significant threat to millions of lives globally (1,2). Unfortunately, many patients with liver malignancies face ineligibility for resection due to medical complexities, an overwhelming disease burden, or insufficient residual liver function. Recent technological advancements in target definition, treatment planning, and setup verification have propelled stereotactic body radiotherapy (SBRT) as an alternative to liver cancer (3-5). SBRT requires accurate radiation delivery to the target while minimizing exposure to surrounding healthy tissues (6,7). The average superior to inferior motion amplitude of the liver during radiation therapy has been shown to be 13 mm, which could add large uncertainties in treatment delivery (8-10). Various maneuvers, including deep inspiration breath-holding (DIBH), free-breathing (FB) using an internal target volume (ITV) strategy based on four-dimensional computed tomography (4D CT), and tracking, are employed in clinical practice to mitigate respiratory motion. Presently, indirect methods such as moving phantoms or machine records have been utilized to estimate targeting accuracy (11,12). Although these methods can indirectly verify the accuracy of treatment, our aim is to validate the overall treatment accuracy of respiratory motion management through the patient's local response of post-radiotherapy.

In clinical practice, contrast-enhanced magnetic resonance imaging (CE-MRI) serves not only in hepatocellular carcinoma (HCC) diagnosis but also as a valuable tool for assessing radiation injury in normal liver tissue (13). Radiation-induced liver disease (RILD) is characterized by elevated liver enzymes and observable morphological alterations on MRI, often occurring after liver SBRT (14). Alterations typically appear hypointense on CE-MRI, signifying veno-occlusive disease in normal liver tissue. Boda-Heggemann *et al.* (15) conducted an *in vivo* analysis (IVA) focusing on treatment accuracies of different motion managements (DIBH and tracking), utilizing the registration of post-radiotherapeutic MRI-morphologic alterations (MMA) to the corresponding planned dose. By 2009, approximately 44% of centers were utilizing 4D CT, highlighting its predominant global usage (16). However, there is no report about IVA regarding the accuracy of liver SBRT using an ITV strategy based on 4D CT.

This study aimed to assess the robustness of accuracy metrics and investigate the impact factors on treatment accuracy of liver SBRT using an ITV strategy based on 4D CT. We present this article in accordance with the STROBE reporting checklist (available at https://qims.amegroups.com/article/view/10.21037/qims-24-2309/rc).

Methods

Patient eligibility

A total of 31 liver SBRT patients treated with FB using an ITV strategy based on 4D CT with additional cone-beam CT (CBCT) monitoring from October 2018 to March 2024 were included in this retrospective study. The study was conducted in accordance with the Declaration of Helsinki and its subsequent amendments. The study was approved by the Ethics Committee of West China Hospital of Sichuan University (No. 2019[430]) and the requirement for individual consent for this retrospective analysis was waived. Patients were

Table 1 Patient, tumor, and treatment characteristics

Variables	Data
Total	31
Gender	
Male	31 (100.0)
Female	0 (0.0)
Age at treatment (years)	51 [33–71]
Karnofsky index (%)	90 [70–100]
Primary tumor	
HCC	29 (93.5)
Else	2 (6.5)
BCLC (n=29)	
0/A/B	10 (34.5)
C	19 (65.5)
Hepatitis virus	
HBV	28 (90.3)
HCV	1 (3.2)
Else	2 (6.5)
TACE	
+	18 (58.1)
–	13 (41.9)
Liver volume at pCT (cc)	1,256.4 [791.7–2,783.9]
GTV (cc)	109.6 [1.0–1,637.4]
PTV (cc)	208.4 [8.55–1,964.8]
GI	3.7 [2.3–9.4]
CN	0.8 [0.4–1]
HI	1.4 [1.1–5.9]
PTV prescription BED (Gy10)	72 [59.5–105.6]
Mean liver EQD2 (Gy3)	88 [70–144]
Time to post-therapeutic MRI (weeks)	21.1 [5.3–50.0]

Data are presented as number, number (%), or median [range]. BCLC, Barcelona Clinic Liver Cancer; BED, biological equivalent dose; CN, conformity number; EQD2, equivalent dose in 2 Gy fractions; GI, gradient index; GTV, gross tumor volume; HBV, hepatitis B virus; HCC, hepatocellular carcinoma; HCV, hepatitis C virus; HI, homogeneity index; MRI, magnetic resonance imaging; pCT, planning computed tomography; PTV, planning target volume; TACE, transarterial chemoembolization.

retrospectively selected in this observational study using the following exclusion criteria: (I) patients without post-therapeutic MRI; (II) MRIs without local morphologic alterations after SBRT; and (III) the area of morphologic alterations caused by transarterial chemoembolization (TACE) overlapping that caused by SBRT. For the treatment protocols, the physical dose was converted to biologically equivalent dose (BED) and equivalent dose in 2 Gy fractions (EQD2) to integrate the treatment protocols. Patient characteristics (age, gender, age at treatment, primary tumor, time to MRI, and so on) are summarized in *Table 1*.

Positioning, planning, and treatment

Patients underwent a 4D CT scan (Revolution ES, GE Healthcare, Milwaukee, WI, USA) for treatment planning. Scans were acquired during quiet breathing without breath coaching under respiratory monitoring (RPM, Varian Medical Systems, Palo Alto, CA, USA). They were positioned supine, with their arms above their head using a body thermoplastic mold with a hole left in the abdomen for the placement of RPM, which was used to collect the patient's respiratory motion amplitude data. In CT simulation, the field of view (FOV) was typically 50 cm, with a slice thickness of 3 mm. The 4D CT data were binned into 10 respiratory phases (T00–T90) with T00 corresponding to the end of inhalation and T50 to the end of exhalation. Gross tumor volume (GTV) was defined based on planning CT and MRI. The ITV was obtained from all the 10 phases. A uniform 5 mm ITV to planning target volume (PTV) margin was expanded around the ITV (the original plan). The average intensity projections (AIP) from 4D CT were adopted for treatment planning and positioning. Treatment planning was performed at a treatment planning system (TPS, Raystation, version 9.0, RaySearch, Stockholm, Sweden).

Patients were treated using a linear accelerator with 6 MV photons (Elekta Versa HD, Elekta Medical Systems, Stockholm, Sweden) with CBCT. CBCT scanning was performed following the patient setup to correct for liver inter-fractional errors in each fraction. Liver shape on pre-correction CBCT scans was aligned with simulation CT scans through manual registration. All liver position alignments were conducted online, with rotational

adjustments neglected. None of the patients had undergone implantation of fiducial markers or stents.

Registration post-radiotherapeutic MRI to planning CT

Transversal, post-radiotherapeutic gadolinium-based T1-weighted sequences CE-MRI were adopted for MMA delineations. Morphologic response assessments were conducted based on post-radiotherapeutic MRI obtained at a median follow-up of 21.3 weeks (range, 5.3–50.0 weeks). The deformable imaging registration was performed using hybrid deformable registration with controlling region of interest (ROI) of liver in discarding image information. Therefore, the contour of the liver in MRI should be performed first. For the selection of isodose lines, several isodose lines ranging from 15 to 45 Gy, with a stepwise increase of 0.1 Gy, were generated on the planning CT. Subsequently, rigid registration was performed between the planning CT and the post-therapeutic MRI, followed by deformable registration based on the liver ROI. Finally, the MMA structure on the MRI was mapped to the planning CT, and structural comparisons were made with various isodose lines on the MIM software (MIM Software, MIM Software Inc., Cleveland, OH, USA), yielding accuracy metrics such as Dice similarity coefficient (DSC), Hausdorff distance (HD), and mean distance to agreement (MDA). The isodose line with the highest DSC and the smallest HD was selected as the most appropriate isodose line structure (*Figure 1*). To reduce interobserver variation, both image registration and delineations were conducted by the same individual and subsequently reviewed by experienced radiation oncologists (n=1), radiologists (n=1), and physicists (n=2). Progression-free survival (PFS) of the clinical target volume (CTV) was evaluated by three radiation oncologists according to the modified Response Evaluation Criteria in Solid Tumors (mRECIST) (17). Tumor stage was also assessed based on the Barcelona Clinic Liver Cancer (BCLC) classification by the same oncologists (18). The respiratory motion amplitudes of the liver were obtained using imaging fusion system (MIM software, MIM software Inc.) by measuring the diaphragm apex across 10 phases of the 4D CT.

IVA and dosimetry analysis

For the IVA, the similarity of MMA and isodose-structure cropped to the liver (ISL) was evaluated in MIM software by the following parameters: the DSC (range, 0–1): structure similarity by considering overlap and union volumes (19,20), HD: the maximum distance between the nearest points of two contours (21). In addition, MDA is the mean surface distance between two contours on registered images (19,22). In contrast to HD, which measures the distance between points that differ the most, MDA finds the mean distance between the two structures. The three-dimensional center-of-mass difference (3D-CoMD) between MMA and ISL was computed and compared to assess the absolute clinical *in vivo* accuracy. Last but not least, we introduced a novel metric of conformity index of MMA and ISL (CIMI) derived from conformity number (CN) to evaluate the similarity of the two structures (23,24). It was described as Eq. [1]:

$$CIMI = \frac{MMA \cap ISL}{MMA} \cdot \frac{MMA \cap ISL}{ISL} \quad [1]$$

Dosimetry metrics including CN, gradient index (GI), and homogeneity index (HI) were used to evaluate the correlation of SBRT plans and accuracy. CN simultaneously takes irradiations of the target volume and healthy tissues into account. A value closer to 1 indicates that the dose distribution fits more tightly to the target volume, preserving healthy tissue. GI is the volume of the 50% isodose line relative to the volume of the prescription isodose line (25). It is adopted to evaluate the speed of which the planning dose falls away from the target volume. HI is the ratio of the maximum dose ($D_{2\%}$) to the minimum dose ($D_{98\%}$) (23). The lower (closer to one) the index, the better the dose homogeneity.

Statistical evaluation

All statistical evaluations were performed using R 4.4.1 (R Foundation for Statistical Computing, Vienna, Austria). The Shapiro-Wilk normality test was used to assess the normality of all data. The consistency between variables and accuracy metrics was evaluated following the normality tests. Data meeting the criteria for normal distribution underwent Pearson correlation analysis, whereas data not meeting these criteria were analyzed using Spearman correlation. The receiver operating characteristic (ROC) curve was employed to determine the cutoffs for the optimal timing of post-therapeutic MRI.

For survival analysis, the endpoint was tumor PFS of CTV radiated, calculated from the time of SBRT to the date of local recurrence (LR) within CTV. The PFS of CTV was calculated using the Kaplan-Meier method and log-rank test. The presence of LR within the CTV was

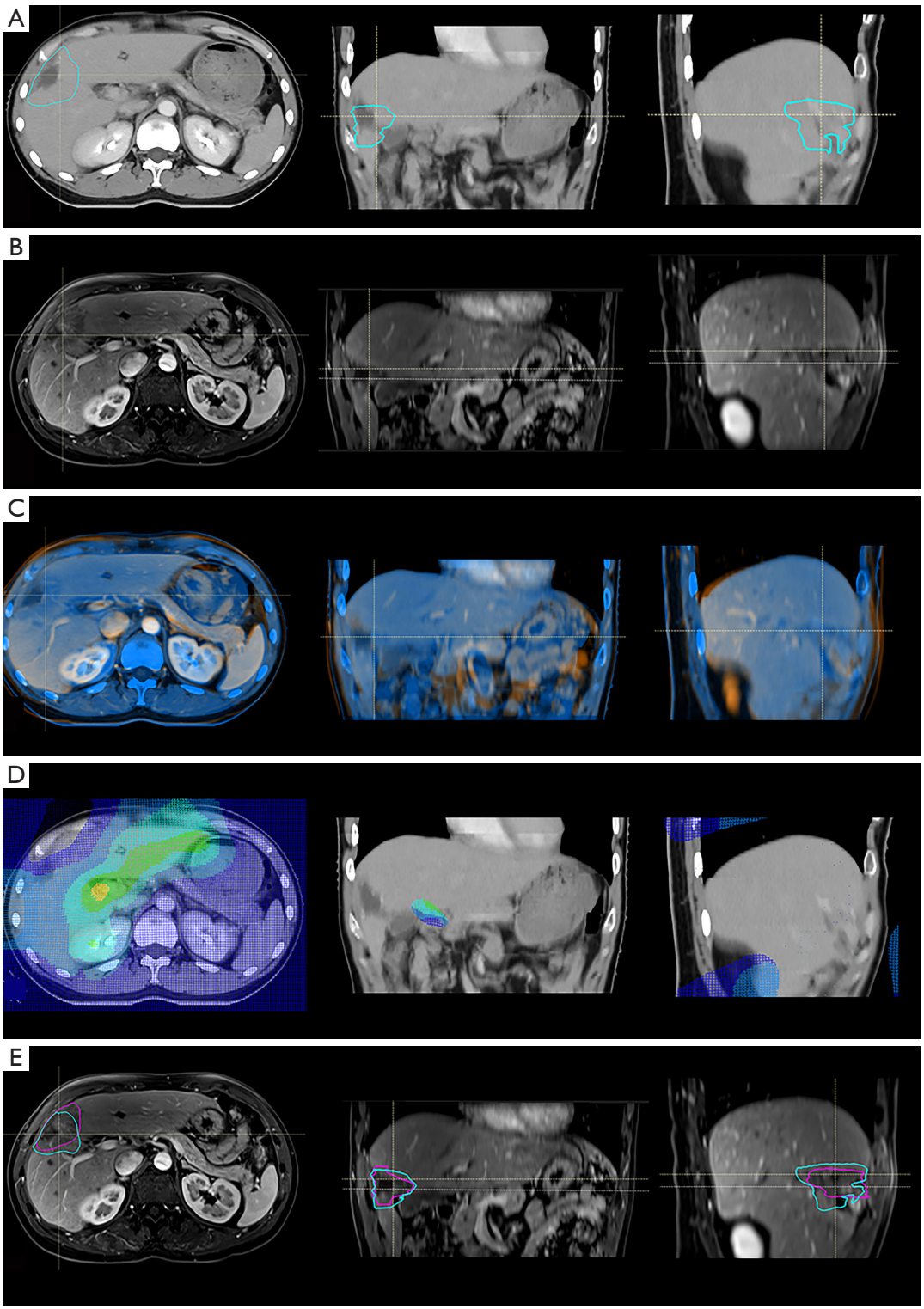

Figure 1 Patient example of 4D CT. (A) Planning CT with ISL of 35.6 Gy; (B) post-radiotherapeutic MRI with hypo-intense alteration; (C) deformable registration of planning CT and post-radiotherapeutic MRI; (D) deformable registration with deform grid; (E) post-radiotherapeutic MRI with mapped ISL of 35.6 Gy. 4D, four-dimensional; CT, computed tomography; ISL, isodose-structure cropped to the liver; MRI, magnetic resonance imaging.

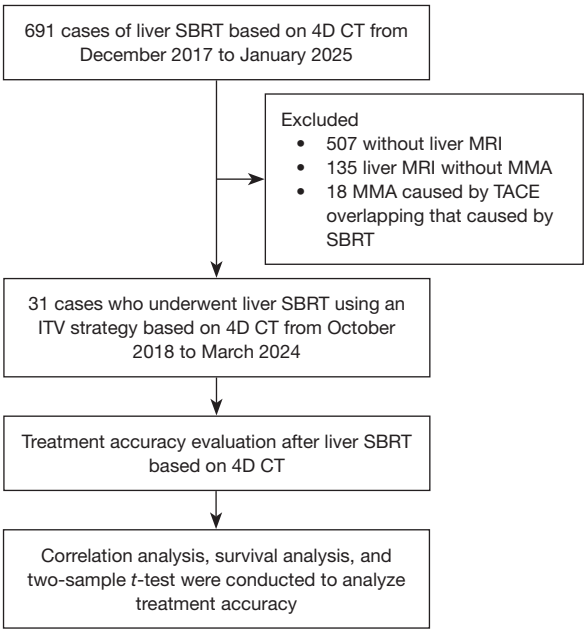

Figure 2 Flowchart of the study design and patient selection process. 4D, four-dimensional; CT, computed tomography; ITV, internal target volume; MMA, MRI-morphologic alterations; MRI, magnetic resonance imaging; SBRT, stereotactic body radiotherapy; TACE, transarterial chemoembolization.

Table 2 Results of IVA after SBRT with 4D CT

Factors	Data
Changed liver volume (cc)	−40.8±195.4 [−7.9]
MMA volume (cc)	228.3±233.5 [134.4]
ISL volume (cc)	313.5±302 [212.3]
ISL (Gy)	31.6±8 [32.4]
DSC	0.7±0.1 [0.7]
CIMI	0.5±0.1 [0.5]
HD (mm)	30±14.1 [26.9]
MDA (mm)	5.4±2.9 [4.9]
3D-CoMD (mm)	9.4±6 [8]
Motion amplitude (mm)	12.5±4.3 [12.4]

Data are presented as mean ± standard deviation [median]. 3D-CoMD, three-dimensional center-of-mass differences; 4D, four-dimensional; CIMI, conformity index of MMA and ISL; CT, computed tomography; DSC, Dice similarity coefficient; HD, Hausdorff distance; ISL, isodose-structure cropped to liver; IVA, in vivo analysis; MDA, mean distance to agreement; MMA, MRI-morphologic alterations; MRI, magnetic resonance imaging; SBRT, stereotactic body radiotherapy.

assessed by two radiation oncologists. Baseline analysis was conducted using the two-sample *t*-test, the two-sample Wilcoxon signed rank test for continuous variables, and the Fisher exact test for categorical variables.

Respiratory motion amplitude of two groups divided by accuracy metrics was analyzed using two-sample *t*-test following Levene's test for homogeneity of variance. After sorting the DSC in ascending order, patients were divided into a low accuracy group and a high accuracy group based on a DSC threshold of 0.7 from the American Association of Physicists in Medicine (AAPM) task group 132 (19). HD, MDA, and 3D-CoMD were similarly divided into two groups according to survival analysis after having been sorted in ascending order.

For all comparisons, $P<0.05$ was considered statistically significant.

Results

Clinical characteristics

We included 31 eligible liver cancer patients who underwent liver SBRT using an ITV strategy based on 4D CT. *Figure 2* presents the study flowchart. Liver volume showed a reduction of −40.8±195.4 (median, −7.9) cc. On contrast-enhanced T1-weighted MRI, MMA appeared hyperintense in 7 cases (23%) and hypointense in 24 cases (77%), consistent with previously published observations (13). The DSC was 0.7±0.1 (median, 0.7). The CIMI for both structures was 0.5±0.1 (median, 0.5). Median value for the MDA was 4.9 mm and for HD was 26.9 mm. Additionally, the median absolute 3D-CoMD measured was 8 mm (*Tables 2*,*3*).

Factors influencing in vivo accuracy

The *in vivo* accuracy was analyzed by conformity metrics (DSC, CIMI), surface-distance metrics (HD, MDA), and 3D-CoMD. According to the correlation test, distance metrics were significantly influenced by GTV, PTV, and time to post-therapeutic MRI (*Table 4*). GI significantly influenced HD (r=−0.438, P=0.014) and MDA (r=−0.431, P=0.016). The conformity metrics (DSC, CIMI) appeared to be more robust than the distance metrics (HD, MDA, 3D-CoMD), as shown in *Table 4*. In the ROC curve analysis of HD, MDA, and 3D-CoMD with respect to the time to post-therapeutic MRI, the area under the curve (AUC) for MDA was 0.765, exceeding that of HD (0.729) and

Table 3 Accuracy metrics, motion amplitude, and treatment plan parameters of patients

Patient	Motion (mm)	DSC	CIMI	HD (mm)	MDA (mm)	3D-CoMD (mm)
1	5.1	0.60	0.38	23.04	5.54	8.78
2	6.6	0.81	0.66	54.10	5.12	7.25
3	6.9	0.27	0.09	78.10	16.72	31.21
4	7.1	0.49	0.29	26.90	7.00	16.75
5	7.4	0.70	0.50	16.38	3.78	6.98
6	7.5	0.61	0.39	29.99	7.19	13.48
7	7.6	0.83	0.70	22.11	4.05	5.63
8	9.3	0.75	0.57	19.80	3.69	5.70
9	9.7	0.63	0.39	27.71	3.87	8.38
10	9.7	0.43	0.25	51.82	12.21	22.52
11	9.8	0.78	0.60	35.87	4.42	9.28
12	10.7	0.65	0.44	13.28	3.20	7.08
13	11.1	0.75	0.57	41.83	8.23	15.80
14	12.2	0.80	0.65	6.83	1.86	1.23
15	12.3	0.68	0.49	32.98	6.62	9.72
16	12.4	0.71	0.51	34.37	5.51	11.02
17	12.8	0.64	0.41	38.46	5.56	10.30
18	13.2	0.64	0.40	14.28	2.64	5.47
19	13.5	0.79	0.62	29.87	3.54	3.82
20	14.2	0.55	0.33	37.52	7.61	7.96
21	14.5	0.71	0.50	24.50	3.89	6.72
22	15.3	0.79	0.62	18.22	3.20	4.78
23	15.5	0.71	0.53	19.98	4.09	4.60
24	16.9	0.71	0.51	24.80	3.35	7.47
25	17.3	0.65	0.53	26.62	5.92	8.71
26	17.6	0.78	0.61	47.51	5.50	13.72
27	17.7	0.85	0.73	35.06	3.13	3.39
28	17.8	0.77	0.60	28.07	5.05	7.76
29	18.1	0.70	0.52	23.81	4.91	10.25
30	19.3	0.49	0.26	25.78	6.73	13.18
31	19.8	0.79	0.62	20.40	3.43	3.37

3D-CoMD, three-dimensional center-of-mass differences; CIMI, conformity index of MMA and ISL; DSC, Dice similarity coefficient; HD, Hausdorff distance; ISL, isodose-structure cropped to liver; MDA, mean distance to agreement; MMA, MRI-morphologic alterations; MRI, magnetic resonance imaging.

Table 4 Statistical analysis of accuracy metrics using Pearson's correlation and Spearman's correlation

Parameters	DSC (MMA and ISL)	CIMI (MMA and ISL)	HD (MMA and ISL)	MDA (MMA and ISL)	3D-CoMD (MMA and ISL)
GTV	0.848	0.863	0.007*	0.003*	0.015*
PTV	0.668	0.654	0.001*	0.003*	0.025*
Prescription	0.647	0.750	0.425	0.523	0.759
BED	0.670	0.805	0.515	0.530	0.854
Liver EQD2	0.628	0.812	0.431	0.414	0.729
Liver volume	0.377	0.291	0.041*	0.066	0.443
Changed liver volume	0.163	0.182	0.470	0.082	0.216
Motion	0.667	0.200	0.451	0.402	0.437
GI	0.540	0.420	0.014*	0.016*	0.060
CN	0.749	0.712	0.868	0.908	0.996
HI	0.736	0.866	0.756	0.814	0.857
Time to post-therapeutic MRI	0.187	0.137	0.009*	0.004*	0.003*

*, P values, statistically significant. 3D-CoMD, three-dimensional center-of-mass differences; BED, biological equivalent dose; CIMI, conformity index of MMA and ISL; CN, conformity number; DSC, Dice similarity coefficient; EQD2, equivalent dose in 2 Gy fractions; GI, gradient index; GTV, gross tumor volume; HD, Hausdorff distance; HI, homogeneity index; ISL, isodose-structure cropped to liver; MDA, mean distance to agreement; MMA, MRI-morphologic alterations; MRI, magnetic resonance imaging; PTV, planning target volume.

Table 5 Characteristics of the patients at baseline grouped by DSC

Characteristics	DSC <0.7	DSC ≥0.7	P value
Gender (male/female)	13/0	18/0	>0.99
Age at treatment (years)	54.62±10.51	53.56±7.62	0.747
GTV (cc)	223.46±322.16	208.82±376.96	0.911
PTV (cc)	328.24±363.71	384.51±457.61	0.718
PTV liver ratio	0.22±0.22	0.25±0.19	0.77
Primary tumor			0.168
HCC	11 (84.6)	18 (100.0)	
Else	2 (15.4)	0 (0.0)	
HBV			0.558
+	11 (84.6)	17 (94.4)	
–	2 (15.4)	1 (5.6)	
TACE			0.727
+	7 (53.8)	11 (61.1)	
–	6 (46.2)	7 (38.9)	
BCLC			0.696
0/A/B	5 (45.5)	6 (33.3)	
C	6 (54.5)	12 (66.7)	

Data of quantitative variables are presented as mean ± standard deviation, while qualitative variables are presented as number or number (%). BCLC, Barcelona Clinic Liver Cancer; DSC, Dice similarity coefficient; GTV, gross tumor volume; HBV, hepatitis B virus; HCC, hepatocellular carcinoma; PTV, planning target volume; TACE, transarterial chemoembolization.

3D-CoMD (0.623). The optimal time to post-therapeutic MRI of MDA was deemed to be 12.4 weeks based on the cutoff.

Clinical outcomes

The median follow-up duration was 37.6 months (range, 9.7–76.2 months) at the time of the last assessment. Among patients with DSC exceeding 0.7, the median PFS of CTV was significantly longer than that of patients with a lower DSC (median PFS, 12 months; log-rank P=0.013). Baseline matching of DSC is shown in *Table 5*, for which there were no significant difference. In the high DSC accuracy group, three patients experienced LR in the CTV, all of whom were classified as BCLC stage C. There was no significant difference between group CIMI less than 0.5 and group CIMI greater than 0.5. For patients with 3D-CoMD greater than 8 mm, HD exceeding 25 mm, and MDA greater than 5 mm, the median PFS were 14 months,12 months, and 14 months, respectively, which were significantly shorter than those with lower 3D-CoMD, HD, and MDA (log-rank P=0.022, log-rank P=0.001, and log-rank P=0.009) (*Figure 3*).

Respiratory motion amplitude difference of metrics

The respiratory motion amplitude of the liver showed

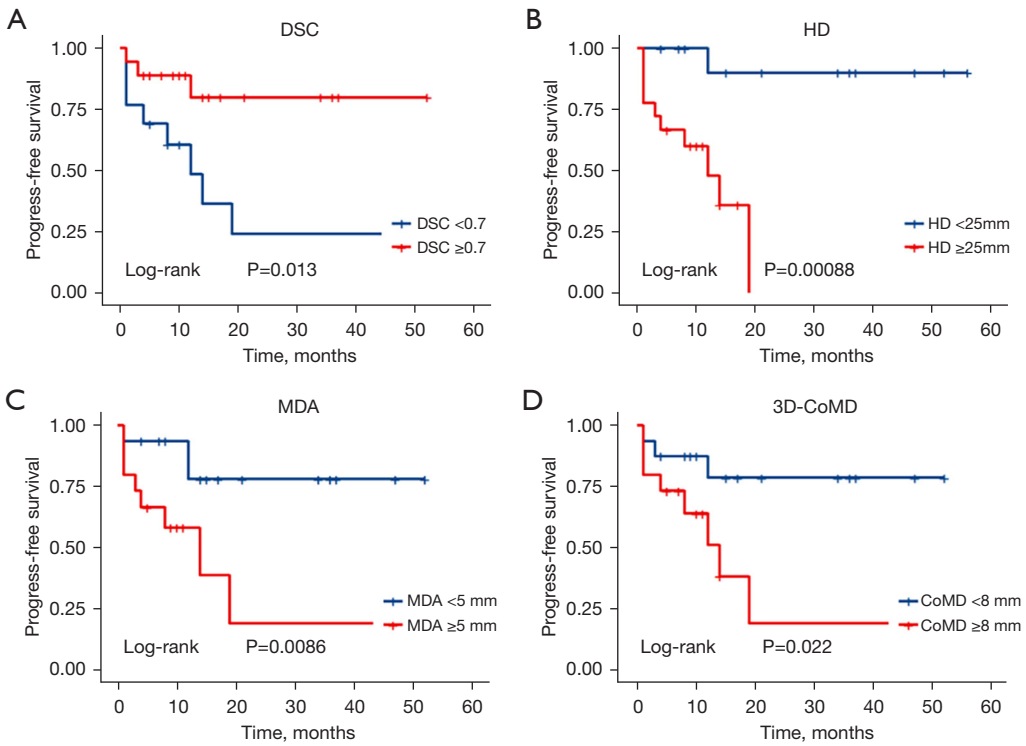

Figure 3 Kaplan-Meier plot. (A) PFS of DSC; (B) PFS of HD; (C) PFS of MDA; (D) PFS of 3D-CoMD. 3D-CoMD, three-dimensional center-of-mass difference; DSC, Dice similarity coefficient; HD, Hausdorff distance; MDA, mean distance to agreement; PFS, progression-free survival.

a median of 12.4 mm in the superior-inferior direction, which is very close to the 13 mm reported in previous studies (26). Accuracy metrics have significant differences in PFS within CTV and were used to compare the motion amplitude of low- and high-accuracy groups. The P value of motion amplitude in the group with DSC lower than 0.7 and group with DSC higher than 0.7 was 11.2 and 13.5 mm, respectively, showing no significant difference. The cutoffs and P values of CIMI, HD, MDA, and 3D-CoMD are presented in *Table 6*, all of which showed no significant difference.

Discussion

The median DSC of both structures was 0.7 in our results, compared to >0.8 in the study by Boda-Heggemann (15). We approach their data cautiously, as only four cases in our dataset achieved a DSC of 0.8 with a similar sample size. This discrepancy may also stem from differences in respiratory motion management. In the consistency test, conformity metrics (DSC, CIMI) were more robust than the distance metrics, including HD, MDA, and 3D-CoMD. Boda-Heggemann reported that the GTV and PTV significantly influenced DSC rather than MDA and 3D-CoMD, which is different from our results.

In analyzing the survival outcomes of patients, significant differences in PFS within CTV were observed with DSC, HD, MDA, and 3D-CoMD (*Figure 2*). The P value for the difference between the high accuracy group and the low accuracy group based on CIMI was 0.08. Survival analysis revealed that patients with a DSC lower than 0.7 had a significantly lower PFS (log-rank P=0.013) than those with higher DSC values. Despite being restricted by the small sample size, the survival outcome still showed that patients' PFS within CTV in the group with a DSC more than 0.7 was significantly better than that of those in the lower accuracy group with a DSC less than 0.7. This means that the higher accuracy of the treatment response (post-radiotherapeutic MMA and corresponding isodose-structure) resulted in higher patients' PFS within CTV. Furthermore, the DSC may be the potentially suitable prognostic predictor for PFS among all accuracy metrics.

Table 6 *T*-test between high/low accuracy and motion amplitude

Metrics (two-sample *t*-test)	Motion amplitude	
	Mean (mm)	P value
DSC		0.142
<0.7	11.2	
≥0.7	13.5	
CIMI		0.055
<0.5	10.7	
≥0.5	13.7	
HD		0.834
<25 mm	12.7	
≥25 mm	12.4	
MDA		0.385
<5 mm	13.2	
≥5 mm	11.8	
3D-CoMD		0.341
<8 mm	13.3	
≥8 mm	11.8	

3D-CoMD, three-dimensional center-of-mass differences; CIMI, conformity index of MMA and ISL; DSC, Dice similarity coefficient; HD, Hausdorff distance; ISL, isodose-structure cropped to liver; MDA, mean distance to agreement; MMA, MRI-morphologic alterations; MRI, magnetic resonance imaging.

Previous studies have reported that the ITV strategy as an effective method of motion management (27,28). However, Dhont *et al.* (29) reported that amplitude changes over 5 mm were 53% for the inter-fraction and 28% for the intra-fraction. Ge *et al.* (30) also stated that 4D CT could not adequately represent the actual motion of abdominal tumors in radiation therapy delivery, especially for SBRT patients. Zeng *et al.* (31) reported that treatment accuracy could also be influenced by intra-fractional liver position baseline shifts. In our study, neither the correlation analysis between motion amplitude and accuracy metrics nor the two-sample *t*-test of motion amplitude showed that motion amplitude had not influenced the accuracy of the treatment response (DSC, HD, MDA, 3D-CoMD). This indicated that patients with larger respiratory motion amplitudes may also exhibit high accuracy, whereas those with smaller ones may demonstrate lower treatment response accuracy. We consider the following reasons may explain this result: (I) for some cases with lower motion amplitude, the ITV may not be accurate because the 4D CT is a snapshot image. (II) The motion amplitude will be changed in the following treatment fractions. (III) The respiratory baseline will be drifted, and the motion amplitude will be altered during dose delivery. Based on these findings, we suggest that a quality assurance procedure in dose delivery should be applied for the ITV strategy based on 4D CT, such as intra-fractional CBCT, fluoroscopy, and MRI image-guided radiotherapy.

Existing literature presents divergent views on the threshold dose (TD) for the MMA post-SBRT in HCC patients with chronic liver disease (32-37). Sanuki *et al.* (38) propose 30 Gy for Child-Pugh (CP)-A disease and 25 Gy for CP-B disease in five fractions as TD, whereas Boda-Heggemann *et al.* (15) identified a TD of 20–21 Gy, which induces centroid morphologic alterations surrounding the lesions. Our study revealed a TD of 31.6±8 (median, 32.4) Gy for 4D CT. Our results appear to be higher than some published observations (15,38); however, Sun *et al.* (36) reported that their median TD was 34.4 Gy, very close to our data of median TD at 32.4 Gy. These TDs hold potential for predicting loss of liver tissue after SBRT (38). The observed significant correlation between GI and MDA could be explained as 50% of the prescribed dose falls within the range of 17.5 to 28 Gy, indicating a trend closely approaching the TD (median, 32.4 Gy). Moreover, it is worth noting that higher DSC may indicate more reliable TDs. Interestingly, the majority of patients in that literature (36) and our cohort are predominantly infected with the hepatitis B virus (HBV), comprising over three-quarters of the cases. Moreover, we are not sure of the reliability of these results, the confirmation of which requires further investigation.

This study has some limitations that should be acknowledged. Firstly, small sample sizes may introduce selection bias, making the results difficult to generalize to a broader population and diminishing statistical power, potentially leading to false positives. Secondly, we employed a single-center, retrospective design, which introduces a possibility of bias, so the results must be validated in multicenter studies. Third, the potential influence of changed liver volume on deformable registration quality may influence the results. To verify the importance of the precision in radiotherapy, a larger sample size and longer follow-up period are needed. Comparisons of treatment accuracy among various respiratory motion management techniques, such as 4D CT, DIBH, and tracking, are also essential. To address these limitations, we plan to include a

larger cohort and conduct a multi-center collaborative study in our forthcoming prospective research.

Conclusions

Conformity metrics such as the DSC and CIMI are more robust than HD, MDA, and 3D-CoMD. For patients undergoing liver SBRT, treatment accuracy has an impact on the PFS in CTV, highlighting the importance of accuracy assurance in radiotherapy. Overall, DSC and CIMI might be the most suitable indicators for predicting PFS within CTV. However, motion amplitude cannot affect the DSC and CIMI. That means a quality assurance procedure in dose delivery should be applied for the ITV strategy based on 4D CT. In addition, we speculate that for patients with liver cancer who are infected by HBV, 32.4 Gy may be the TD.

Acknowledgments

None.

Footnote

Reporting Checklist: The authors have completed the STROBE reporting checklist. Available at https://qims.amegroups.com/article/view/10.21037/qims-24-2309/rc

Funding: This work was supported by the Science and Technology Department of Sichuan Province, China (No. 2024YFFK0147), the National Natural Science Foundation of China (No. 12405390), and the Natural Science Foundation of Sichuan Province (No. 2023NSFSC1319).

Conflicts of Interest: All authors have completed the ICMJE uniform disclosure form (available at https://qims.amegroups.com/article/view/10.21037/qims-24-2309/coif). M.G. is from GE Healthcare. The other authors have no conflicts of interest to declare.

Ethical Statement: The authors are accountable for all aspects of the work in ensuring that questions related to the accuracy or integrity of any part of the work are appropriately investigated and resolved. The study was conducted in accordance with the Declaration of Helsinki and its subsequent amendments. The study was approved by the Ethics Committee of West China Hospital of Sichuan University (No. 2019[430]) and the requirement for individual consent for this retrospective analysis was waived.

References

1. Sung H, Ferlay J, Siegel RL, Laversanne M, Soerjomataram I, Jemal A, Bray F. Global Cancer Statistics 2020: GLOBOCAN Estimates of Incidence and Mortality Worldwide for 36 Cancers in 185 Countries. CA Cancer J Clin 2021;71:209-49.
2. Horn SR, Stoltzfus KC, Lehrer EJ, Dawson LA, Tchelebi L, Gusani NJ, Sharma NK, Chen H, Trifiletti DM, Zaorsky NG. Epidemiology of liver metastases. Cancer Epidemiol 2020;67:101760.
3. Price TR, Perkins SM, Sandrasegaran K, Henderson MA, Maluccio MA, Zook JE, Tector AJ, Vianna RM, Johnstone PA, Cardenes HR. Evaluation of response after stereotactic body radiotherapy for hepatocellular carcinoma. Cancer 2012;118:3191-8.
4. Huang WY, Jen YM, Lee MS, Chang LP, Chen CM, Ko KH, Lin KT, Lin JC, Chao HL, Lin CS, Su YF, Fan CY, Chang YW. Stereotactic body radiation therapy in recurrent hepatocellular carcinoma. Int J Radiat Oncol Biol Phys 2012;84:355-61.
5. Kim N, Cheng J, Jung I, Liang J, Shih YL, Huang WY, Kimura T, Lee VHF, Zeng ZC, Zhenggan R, Kay CS, Heo SJ, Won JY, Seong J. Stereotactic body radiation therapy vs. radiofrequency ablation in Asian patients with hepatocellular carcinoma. J Hepatol 2020;73:121-9.
6. Sharma M, Nano TF, Akkati M, Milano MT, Morin O, Feng M. A systematic review and meta-analysis of liver tumor position variability during SBRT using various motion management and IGRT strategies. Radiother Oncol 2022;166:195-202.
7. Van den Begin R, Engels B, Gevaert T, Duchateau M, Tournel K, Verellen D, Storme G, De Ridder M. Impact of inadequate respiratory motion management in SBRT for oligometastatic colorectal cancer. Radiother Oncol 2014;113:235-9.

8. Nierer L, Eze C, da Silva Mendes V, Braun J, Thum P, von Bestenbostel R, Kurz C, Landry G, Reiner M, Niyazi M, Belka C, Corradini S. Dosimetric benefit of MR-guided online adaptive radiotherapy in different tumor entities: liver, lung, abdominal lymph nodes, pancreas and prostate. Radiat Oncol 2022;17:53.
9. Nankali S, Worm ES, Hansen R, Weber B, Høyer M, Zirak A, Poulsen PR. Geometric and dosimetric comparison of four intrafraction motion adaptation strategies for stereotactic liver radiotherapy. Phys Med Biol 2018;63:145010.
10. Stera S, Miebach G, Buergy D, Dreher C, Lohr F, Wurster S, Rödel C, Marcella S, Krug D, Frank A G, Ehmann M, Fleckenstein J, Blanck O, Boda-Heggemann J. Liver SBRT with active motion-compensation results in excellent local control for liver oligometastases: An outcome analysis of a pooled multi-platform patient cohort. Radiother Oncol 2021;158:230-6.
11. Jung J, Song SY, Yoon SM, Kwak J, Yoon K, Choi W, Jeong SY, Choi EK, Cho B. Verification of Accuracy of CyberKnife Tumor-tracking Radiation Therapy Using Patient-specific Lung Phantoms. Int J Radiat Oncol Biol Phys 2015;92:745-53.
12. Klein TJ, Gill S, Ebert MA, Grogan G, Smith W, Alkhatib Z, Geraghty J, Scott AJD, Brown A, Rowshanfarzad P. CyberKnife Xsight versus fiducial-based target-tracking: a novel 3D dosimetric comparison in a dynamic phantom. Radiat Oncol 2022;17:154.
13. Dreher C, Sarria GR, Miebach G, Weiss C, Buergy D, Wojtal P, Tavakoli AA, Krug D, Oppitz H, Giordano FA, Both M, Lohr F, Dunst J, Blanck O, Boda-Heggemann J. Long-term characterization of MRI-morphologic alterations after active motion-compensated liver SBRT: a multi-institutional pooled analysis. Acta Oncol 2023;62:281-9.
14. Olsen CC, Welsh J, Kavanagh BD, Franklin W, McCarter M, Cardenes HR, Gaspar LE, Schefter TE. Microscopic and macroscopic tumor and parenchymal effects of liver stereotactic body radiotherapy. Int J Radiat Oncol Biol Phys 2009;73:1414-24.
15. Boda-Heggemann J, Jahnke A, Chan MKH, Ernst F, Ghaderi AL, Attenberger U, Hunold P, Schäfer JP, Wurster S, Rades D, Hildebrandt G, Lohr F, Dunst J, Wenz F, Blanck O. In-vivo treatment accuracy analysis of active motion-compensated liver SBRT through registration of plan dose to post-therapeutic MRI-morphologic alterations. Radiother Oncol 2019;134:158-65.
16. Simpson DR, Lawson JD, Nath SK, Rose BS, Mundt AJ, Mell LK. Utilization of advanced imaging technologies for target delineation in radiation oncology. J Am Coll Radiol 2009;6:876-83.
17. Llovet JM, Lencioni R. mRECIST for HCC: Performance and novel refinements. J Hepatol 2020;72:288-306.
18. Reig M, Forner A, Rimola J, Ferrer-Fàbrega J, Burrel M, Garcia-Criado Á, Kelley RK, Galle PR, Mazzaferro V, Salem R, Sangro B, Singal AG, Vogel A, Fuster J, Ayuso C, Bruix J. BCLC strategy for prognosis prediction and treatment recommendation: The 2022 update. J Hepatol 2022;76:681-93.
19. Brock KK, Mutic S, McNutt TR, Li H, Kessler ML. Use of image registration and fusion algorithms and techniques in radiotherapy: Report of the AAPM Radiation Therapy Committee Task Group No. 132. Med Phys 2017;44:e43-76.
20. Dice LR. Measures of the amount of ecologic association between species. Ecology 1945;26:297-302.
21. Munkres JR. Topology. 2nd ed. Upper Saddle River: Prentice Hall Inc.; 2000.
22. Chalana V, Kim Y. A methodology for evaluation of boundary detection algorithms on medical images. IEEE Trans Med Imaging 1997;16:642-52.
23. Feuvret L, Noël G, Mazeron JJ, Bey P. Conformity index: a review. Int J Radiat Oncol Biol Phys 2006;64:333-42.
24. van't Riet A, Mak AC, Moerland MA, Elders LH, van der Zee W. A conformation number to quantify the degree of conformality in brachytherapy and external beam irradiation: application to the prostate. Int J Radiat Oncol Biol Phys 1997;37:731-6.
25. Paddick I, Lippitz B. A simple dose gradient measurement tool to complement the conformity index. J Neurosurg 2006;105 Suppl:194-201.
26. Brandner ED, Wu A, Chen H, Heron D, Kalnicki S, Komanduri K, Gerszten K, Burton S, Ahmed I, Shou Z. Abdominal organ motion measured using 4D CT. Int J Radiat Oncol Biol Phys 2006;65:554-60.
27. Heinzerling JH, Anderson JF, Papiez L, Boike T, Chien S, Zhang G, Abdulrahman R, Timmerman R. Four-dimensional computed tomography scan analysis of tumor and organ motion at varying levels of abdominal compression during stereotactic treatment of lung and liver. Int J Radiat Oncol Biol Phys 2008;70:1571-8.
28. Xu H, Gong G, Yin Y, Liu T. A preliminary investigation of re-evaluating the irradiation dose in hepatocellular carcinoma radiotherapy applying 4D CT and deformable registration. J Appl Clin Med Phys 2021;22:13-20.
29. Dhont J, Vandemeulebroucke J, Burghelea M, Poels K, Depuydt T, Van Den Begin R, Jaudet C, Collen C,

Engels B, Reynders T, Boussaer M, Gevaert T, De Ridder M, Verellen D. The long- and short-term variability of breathing induced tumor motion in lung and liver over the course of a radiotherapy treatment. Radiother Oncol 2018;126:339-46.
30. Ge J, Santanam L, Noel C, Parikh PJ. Planning 4-dimensional computed tomography (4DCT) cannot adequately represent daily intrafractional motion of abdominal tumors. Int J Radiat Oncol Biol Phys 2013;85:999-1005.
31. Zeng L, Wang X, Zhou J, Gong P, Wang X, Wu X, Deng Z, Li B, Liu D, Zhong R. Analysis of the amplitude changes and baseline shifts of respiratory motion using intra-fractional CBCT in liver stereotactic body radiation therapy. Phys Med 2022;93:52-8.
32. Takeda A, Oku Y, Sanuki N, Kunieda E, Koike N, Aoki Y, Ohashi T, Iwabuchi S, Takatsuka K, Takeda T, Sugawara A. Dose volume histogram analysis of focal liver reaction in follow-up multiphasic CT following stereotactic body radiotherapy for small hepatocellular carcinoma. Radiother Oncol 2012;104:374-8.
33. Jung J, Yoon SM, Cho B, Choi YE, Kwak J, Kim SY, Lee SW, Ahn SD, Choi EK, Kim JH. Hepatic reaction dose for parenchymal changes on Gd-EOB-DTPA-enhanced magnetic resonance images after stereotactic body radiation therapy for hepatocellular carcinoma. J Med Imaging Radiat Oncol 2016;60:96-101.
34. Doi H, Shiomi H, Masai N, Tatsumi D, Igura T, Imai Y, Oh RJ. Threshold doses and prediction of visually apparent liver dysfunction after stereotactic body radiation therapy in cirrhotic and normal livers using magnetic resonance imaging. J Radiat Res 2016;57:294-300.
35. Kuznetsova S, Sinha R, Thind K, Ploquin N. Direct visualization and correlation of liver stereotactic body radiation therapy treatment delivery accuracy with interfractional motion. J Appl Clin Med Phys 2021;22:129-38.
36. Sun XL, Jiang X, Kuang Y, Xing L, Bu LY, Yuan SH, Yu JM, Zheng SS. Potential of Gd-EOB-DTPA as an imaging biomarker for liver injury estimation after radiation therapy. Hepatobiliary Pancreat Dis Int 2019;18:354-9.
37. Ebara M, Shibuya K, Shimada H, Kawashima M, Hirasawa H, Taketomi-Takahashi A, Ohno T, Tsushima Y. Evaluation of Threshold Dose of Damaged Hepatic Tissue After Carbon-Ion Radiation Therapy Using Gd-EOB-DTPA-Enhanced Magnetic Resonance Imaging. Adv Radiat Oncol 2021;6:100775.
38. Sanuki N, Takeda A, Oku Y, Eriguchi T, Nishimura S, Aoki Y, Mizuno T, Iwabuchi S, Kunieda E. Threshold doses for focal liver reaction after stereotactic ablative body radiation therapy for small hepatocellular carcinoma depend on liver function: evaluation on magnetic resonance imaging with Gd-EOB-DTPA. Int J Radiat Oncol Biol Phys 2014;88:306-11.

Cite this article as: Ye H, Chan C, Huang Y, Pu Y, Guo M, Zhang X, Zhang Y, Wang X, Zhou J, Duan J, Wang S, Peng L, Yu H, Tan Q, Zeng X, Zhong R. Assessing treatment accuracy of image-guided liver stereotactic body radiotherapy: a quantitative analysis based on 4D CT through post-therapeutic MRI-morphologic alterations. Quant Imaging Med Surg 2025;15(5):4180-4192. doi: 10.21037/qims-24-2309